Reciprocal Metasurfaces for On-Axis Reflective Optical Computing

Ali Momeni, Hamid Rajabalipanah, Mahdi Rahmanzadeh, Ali Abdolali, Karim Achouri, Viktar S. Asadchy, and Romain Fleury

***Abstract*— Analog computing has emerged as a promising candidate for real-time and parallel continuous data processing. This article presents a reciprocal way for realizing asymmetric optical transfer functions (OTFs) in the reflection side of the on-axis processing channels. It is rigorously demonstrated that the presence of cross-polarization exciting normal polarizabilities (CPENPs) of a reciprocal metasurface circumvents the famous challenge of Green's function approach in implementation of on-axis reflective optical signal processing while providing dual computing channels under orthogonal polarizations. Following a comprehensive theoretical discussion and as a proof of concept, an all-dielectric optical metasurface is elaborately designed to exhibit the desired surface polarizabilities, thereby reflecting the first derivative and extracting the edges of images impinging from the normal direction. The proposed study offers a flexible design method for on-axis metasurface-based optical signal processing and also dramatically facilitates the experimental setup required for ultrafast analog computation and image processing.**

***Index Terms*— All-dielectric metasurfaces, optical signal processing, surface polarizabilities.**

I. Introduction

OVER the past few years, the growing demands for ultrafast and large-scale signal, image, and information system processing as well as the saturation of digital computational capacities have brought about the emergence of new proposals for optical analog computing schemes [1]–[3]. In traditional approaches, mathematical processing is mainly performed in the digital domain by using traditional integrated electronic-based technologies for implementing logics [4]–[7], differentiators, and integrators [8], [9]. Unfortunately, these computing hardwares have some major disadvantages related to operational speed and power consumption [10], [11]. Recently, Silva *et al.* [11] proposed the construction of analog computational metamaterials, based on two distinct approaches: the spatial Fourier transfer and Green's function (GF) methods [12]. The former solution, executed in the spatial Fourier domain, was initially accompanied by additional bulky optical components (4*f* correlators), hindering miniaturization [11], [13]. This shortcoming was later avoided by directly realizing the spatial impulse response of interest by means of the nonlocal transmission or reflection response of artificial structures [14]–[17]. A large number of studies presented resonant and nonresonant structures to expand this idea for advanced all-optical signal processing architectures [18]–[20]. Kwon *et al.* [15] demonstrated that the nonlocality of artificial structures can be engineered to enable signal manipulation in the momentum domain over an ultrathin platform for performing basic mathematical operations in transmission mode. Another progress in this area, discussed in [14], has shown that the interference effects associated with surface plasmon excitations at a single metal–dielectric interface can perform spatial differentiation and edge detection. More recently, a theoretical work has demonstrated that the Laplacian operator required to do spatial differentiation in transmission mode can be obtained using the guided resonances of a photonic crystal slab [21]. Besides, different innovative approaches have also been reported, for instance, manipulating the complex-valued electromagnetic wave propagating through specially designed recursive paths [22] or the use of topological insulators as a way to increase the robustness to geometrical tolerances [23].

In the GF-based optical signal processing methods, the metasurfaces often aim at realizing transfer functions (TFs) with either odd-/or even-symmetric properties [see Fig. 1(a)]. For odd/even TFs, the reflection or transmission coefficient of the metasurface processor should be an asymmetric/symmetric function of the incident angle. Due to fundamental limitations arising from the nonlocal behavior of reflection/transmission responses in the wave-vector domain, the existing GF-based analog computing proposals have exploited complex oblique illumination setups (challenging

Manuscript received December 24, 2020; revised February 24, 2021; accepted April 20, 2021. Date of publication May 14, 2021; date of current version October 28, 2021. The work of Ali Momeni and Romain Fleury was supported by the Swiss National Science Foundation (SNSF) under the Eccellenza Award 181232. *(Corresponding authors: Ali Abdolali; Romain Fleury.)*

Ali Momeni and Romain Fleury are with the Laboratory of Wave Engineering, School of Electrical Engineering, Swiss Federal Institute of Technology in Lausanne (EPFL), 1015 Lausanne, Switzerland (e-mail: romain.fleury@epfl.ch).

Hamid Rajabalipanah and Ali Abdolali are with the Applied Electromagnetic Laboratory, School of Electrical Engineering, Iran University of Science and Technology, Tehran 16846-13114, Iran (e-mail: abdolali@iust.ac.ir).

Mahdi Rahmanzadeh is with the Department of Electrical Engineering, Sharif University of Technology, Tehran 11155-4363, Iran.

Karim Achouri is with the Nanophotonics and Metrology Laboratory, Swiss Federal Institute of Technology Lausanne (EPFL), 1015 Lausanne, Switzerland.

Viktar S. Asadchy is with the Ginzton Laboratory, Stanford University, Stanford, CA 94305 USA, also with the Department of Electrical Engineering, Stanford University, Stanford, CA 94305 USA, and also with the Department of Electronics and Nanoengineering, Aalto University, 00076 Aalto, Finland.

Color versions of one or more figures in this article are available at https://doi.org/10.1109/TAP.2021.3078521.

Digital Object Identifier 10.1109/TAP.2021.3078521

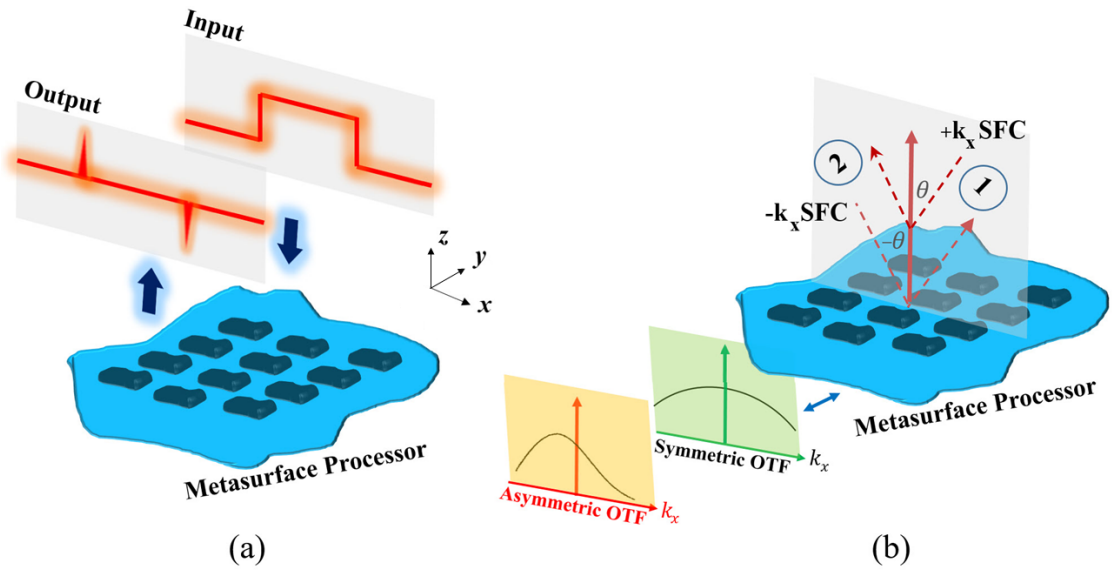

Fig. 1. (a) Schematic sketch of the proposed spatial metasurface processor for performing real-time on-axis reflective analog signal processing. (b) Demonstration of the symmetries/asymmetries of the angular scattering around the boresight direction for nonreciprocal/reciprocal metasurfaces.

to align) to implement odd-symmetric operations [14], [18], [19], [24], [25]. In most practical situations, realizing on-axis signal processing operators with asymmetric optical transfer functions (OTFs) is a key requirement for increasing the compatibility with standard image processing/recognition schemes, such as image sharpening and edge detection [17], [26]–[28]. In addition, reflection-type processing systems are superior to transmission-type ones in terms of compactness. Besides, although using both reflection and transmission channels of the metasurfaces would enhance the degrees of freedom for performing parallel processing, the on-axis reflective channels are still unavailable. The reason is attributed to the fact that realizing an odd-symmetric angular dispersion for copolarized components of these channels violates the well-known reciprocity theorem [29]. Nevertheless, up to now, prior proposals for accomplishing on-axis optical signal processing have only considered transmissive configurations [15], [26], [28]–[32].

Motivated by such theoretical developments, here, we propose a reciprocal way for exploiting the on-axis reflective processing channels in bianisotropic metasurfaces. We demonstrate that considering the cross-polarization reflections caused by the normal polarizabilities of bianisotropic metasurfaces brings in new degrees of freedom in controlling the meta-atom scattering. We reveal a simple appealing opportunity to circumvent the coercive reflection symmetry in the wave-vector domain without resorting to intricate nonreciprocal options or bulky Fourier lenses. We show that using the cross-polarized channels enabled by a certain group of normal polarizabilities, the odd-symmetric operations can be implemented in on-axis reflective scenarios. Compared with recent works [26], [29], [31], [33], the main contributions of this article are as follows.

1) By considering the general form of the surface polarizabilities of a reciprocal bianisotropic metasurface, we extract the general rules for performing standard on-axis optical signal processing tasks in the reflection side. Some remarks about the transmission configuration are also presented.
2) Realizing an all-dielectric optical metasurface that exposes the desired collective polarzabilites and creates a cross-polarized reflective processing channel.

II. Theoretical Investigation

A. Scattering Coefficients of a Metasurface

Fig. 1(a) shows the employed computational metasurface comprising a uniform array of polarizable meta-atoms in the xy plane (z = 0). Let us consider that p-polarized (or s-polarized) light with a transverse field profile of $\mathrm{s_{in}(x)}$ impinges normally on the metasurface processor (along the $-z$-direction). This incident light is reflected by the metasurface with a beam profile $\mathrm{s_{out}(x)}$ in the $+z$-direction. Here, p- and s-polarized refer to the polarized lights whose electric field is oriented along the x- and y-directions, respectively, at normal incidences. In the spatial Fourier domain, each beam profile can be spectrally represented by a superposition of plane waves, as spatial Fourier components (SPFs), i.e., $\mathrm{s_{in}(x)} = \int_{2W} \tilde{s}_{\mathrm{inc}}(k_x)\, \exp(jk_z z + jk_x x)\, dk_x$ and $\mathrm{s_{out}(x)} = \int_{2W} \tilde{H}(k_x)\tilde{s}_{\mathrm{inc}}(k_x)\, \exp(-jk_z z + jk_x x)\, dk_x$. Here, W denotes the spatial bandwidth of the input signal and $\mathrm{k_x} = \mathrm{k_0 sin}\theta$ specifies the x component of the wavenumber of the plane-wave harmonic illuminating the metasurface with the incidence angle θ. Moreover, $\tilde{H}(k_x)$ refers to the TF describing an operator of choice that we aim at synthesizing. Due to the subwavelength periodicity of the metasurface along the x-direction, the tangential wave vector $\mathrm{k_x}$ must be continuous at the interface. Therefore, the incident plane wave with $\mathrm{k_x}$ only generates a reflected propagating plane wave with the same $\mathrm{k_x}$. Furthermore, the beam-profile transformation between the incident and reflected lights can be spectrally described by using a spatially dispersive TF representing the mathematical operator of interest, $\tilde{H}(k_x) = s_{out}(k_x)/s_{in}(k_x)$. Mathematically

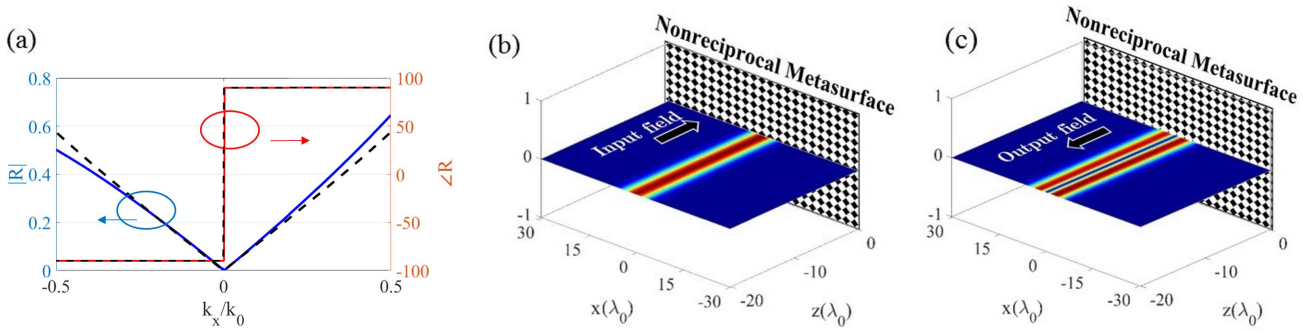

Fig. 2. (a) Synthesized (dashed line) and exact (solid line) TFs obtained by a nonreciprocal anisotropic metasurface differentiator characterized with the following polarizabilities: $\alpha_{\rm ee}^{xx} = 1 \times 10^{-20}$, $\alpha_{\rm ee}^{xz} = 2.73 \times 10^{-17}$, $\alpha_{\rm ee}^{zx} = 2.19 \times 10^{-17}$, $\alpha_{\rm ee}^{zz} = 1.21 \times 10^{-18}$, and $\alpha_{\rm mm}^{yy} = 1 \times 10^{-16}$. All quantities are in $\rm m^3$. (b) Gaussian-shape incident field and (c) derivative reflected field along the boresight direction.

speaking, the k_x-dependence of the TF should be imparted by the angular response of the scattering parameter (reflection or transmission coefficient) of the employed metasurface [34]. It should be noted that the challenges accompanied with reflective optical signal processing of on-axis illuminations are more severe than those of transmissive configurations. For instance, designing asymmetric reflective OTFs by using copolarization channels inherently requires nonreciprocity [29]. Although both reflection and transmission problems will be investigated, the focus of this article is the reflection mode. In this case, the output field of the metasurface processor is $\rm s_{out}(x) = F^{-1}\{s_{inc}(k_x)\tilde{R}(k_x)\}$. The metasurface can be theoretically treated as a bianisotropic homogeneous sheet in its general form with four distinct sets of collective polarizabilities ($\overline{\overline{\hat{\alpha}}}_{\rm ee}$, $\overline{\overline{\hat{\alpha}}}_{\rm em}$, $\overline{\overline{\hat{\alpha}}}_{\rm me}$, and $\overline{\overline{\hat{\alpha}}}_{\rm mm}$) [35]. Keeping the tensorial format of polarizability components in mind, the reflection coefficient (the TF) exerted by the metasurface boundary would be different for s- and p-polarized signals, and we write

$$\overline{\overline{\tilde{H}}}(k_x) \equiv \begin{bmatrix} \tilde{R}^{s\to s}(k_x) & \tilde{R}^{s\to p}(k_x) \\ \tilde{R}^{p\to s}(k_x) & \tilde{R}^{p\to p}(k_x) \end{bmatrix} \tag{1}$$

where $\tilde{R}$ alludes to the nonlocal reflection coefficient of the bianisotropic metasurface in the wave-vector domain. The first and second superscripts refer to the polarization state of the input and output fields, respectively. Indeed, for an arbitrary input signal having a specific polarization state, the bianisotropic metasurface may suggest two possible TFs resulting in two different output signals with s or p polarization in the reflection mode. Each tensorial component of the TF in (1) is affiliated to a certain combination of surface polarizabilities, in an explicit or implicit manner. To unveil these dependencies, we need constitutive parameters that do not change with different conditions of the external excitation and only depend on the physical parameters of the metasurface, i.e., the shapes and sizes of the meta-atoms.

With the advent of metasurfaces, a new generation of 2-D computational interfaces has emerged to spatially shape the optical fields over deeply subwavelength volumes [36]–[38]. Several characterization frameworks based on local tensorial scattering coefficients [39]–[46], surface impedance formulation [47], [48], generalized sheet transition conditions (GSTCs) by susceptibility tensors [49], [50], as well as individual/effective polarizabilities [35], [51]–[53] have been fostered to represent metasurfaces in their general bianisotropic forms. These methods do consider normal components; however, in most studies, the normal components are omitted. However, normal components are pivotal when complex spatially dispersive behavior are demanded in reflection or transmission mode [34]. We thus take these components fully into account and follow the so-called Tretyakov–Simovski formalism relating the fields and polarizations in the general form [35], [52]:

$$\mathbf{p} = \overline{\overline{\hat{\alpha}}}_{\rm ee} \cdot \mathbf{E}_{\rm inc} + \overline{\overline{\hat{\alpha}}}_{\rm em} \cdot \mathbf{H}_{\rm inc} \tag{2}$$

$$\mathbf{m} = \overline{\overline{\hat{\alpha}}}_{\rm me} \cdot \mathbf{E}_{\rm inc} + \overline{\overline{\hat{\alpha}}}_{\rm mm} \cdot \mathbf{H}_{\rm inc} \tag{3}$$

in which $\overline{\overline{\hat{\alpha}}}_{\rm ee}$, $\overline{\overline{\hat{\alpha}}}_{\rm em}$, $\overline{\overline{\hat{\alpha}}}_{\rm me}$, and $\overline{\overline{\hat{\alpha}}}_{\rm mm}$ are called collective surface polarizabilities: electric, magnetoelectric, electromagnetic, and magnetic ones, respectively. $\mathbf{P}$ and $\mathbf{M}$ also represent the electric and magnetic polarization densities induced on the metasurface, respectively. The transversal components of the reflected and transmitted electric fields can be expressed by [52]

$$\begin{aligned} \mathbf{E}_{\rm ref,t} = &-(\overline{\overline{I}}_t + \overline{\overline{Z}}_{bo}^{to}\overline{\overline{Y}}_{to}^{bo})^{-1}(\overline{\overline{I}}_t - \overline{\overline{Z}}_{bo}^{to}\overline{\overline{Y}}_{to}^{bo}) \\ &\cdot \mathbf{E}_{\rm inc,t} - (\overline{\overline{I}}_t + \overline{\overline{Z}}_{bo}^{to}\overline{\overline{Y}}_{to}^{bo})^{-1} \\ &\cdot \Big[j\omega(\overline{\overline{Z}}_{bo}^{to} \cdot \mathbf{P}_t \pm \mathbf{n} \times \mathbf{M}_t) \\ &\pm j\left(\mathbf{k}_t \frac{P_n}{\varepsilon} \mp \overline{\overline{Z}}_{bo}^{to} \cdot (\mathbf{k}_t \times \mathbf{n}) \frac{M_n}{\mu}\right)\Big] \end{aligned} \tag{4}$$

$$\begin{aligned} \mathbf{E}_{\rm tran,t} = &(\overline{\overline{I}}_t + \overline{\overline{Z}}_{to}^{bo}\overline{\overline{Y}}_{bo}^{to})^{-1}(\overline{\overline{I}}_t + \overline{\overline{Z}}_{to}^{bo}\overline{\overline{Y}}_{bo}^{to}) \\ &\cdot \mathbf{E}_{\rm inc,t} - (\overline{\overline{I}}_t + \overline{\overline{Z}}_{to}^{bo}\overline{\overline{Y}}_{bo}^{to})^{-1} \\ &\cdot \Big[j\omega(\overline{\overline{Z}}_{to}^{bo} \cdot \mathbf{P}_t \mp \mathbf{n} \times \mathbf{M}_t) \\ &\mp j\left(\mathbf{k}_t \frac{P_n}{\varepsilon} \pm \overline{\overline{Z}}_{to}^{bo} \cdot (\mathbf{k}_t \times \mathbf{n}) \frac{M_n}{\mu}\right)\Big] \end{aligned} \tag{5}$$

where $\mathbf{P} = \mathbf{p}/S$ and $\mathbf{M} = \mathbf{m}/S$ are polarization surface densities in which S denotes the unit cell area. Also, the top/bottom sign corresponds to the wave propagating along the $\mp z$-direction, and to and bo in the subscripts refer to top/bottom medium, respectively. For the sake of simplicity, we assume that the metasurface is surrounded by

free space. Thus, $\overline{\overline{Z}}$ and $\overline{\overline{Y}} = \overline{\overline{Z}}^{-1}$ denoting, respectively, the dyadic impedance and admittance of the corresponding medium can be written as (6), as shown at the bottom of the page, [54] where η is the free-space impedance and θ and ϕ are the elevation and azimuth angles of the incident wave, respectively. The formulations above may be applied for any special case of external illumination, for example, s- or p- polarized incident waves or a superposition of these two. To exploit the full potential of the metasurface boundary, each polarizability tensor of (2) and (3) includes both normal and tangential components, i.e., 36 scalar polarizabilities, which can be written as

$$\overline{\overline{\alpha}}_{\rm ee} = \begin{bmatrix} \alpha_{\rm ee}^{xx} & \alpha_{\rm ee}^{xy} & \alpha_{\rm ee}^{xz} \\ \alpha_{\rm ee}^{yx} & \alpha_{\rm ee}^{yy} & \alpha_{\rm ee}^{yz} \\ \alpha_{\rm ee}^{zx} & \alpha_{\rm ee}^{zy} & \alpha_{\rm ee}^{zz} \end{bmatrix}, \quad \overline{\overline{\alpha}}_{\rm em} = \begin{bmatrix} \alpha_{\rm em}^{xx} & \alpha_{\rm em}^{xy} & \alpha_{\rm em}^{xz} \\ \alpha_{\rm em}^{yx} & \alpha_{\rm em}^{yy} & \alpha_{\rm em}^{yz} \\ \alpha_{\rm em}^{zx} & \alpha_{\rm em}^{zy} & \alpha_{\rm em}^{zz} \end{bmatrix} \tag{7}$$

$$\overline{\overline{\alpha}}_{\rm me} = \begin{bmatrix} \alpha_{\rm me}^{xx} & \alpha_{\rm me}^{xy} & \alpha_{\rm me}^{xz} \\ \alpha_{\rm me}^{yx} & \alpha_{\rm me}^{yy} & \alpha_{\rm me}^{yz} \\ \alpha_{\rm me}^{zx} & \alpha_{\rm me}^{zy} & \alpha_{\rm me}^{zz} \end{bmatrix}, \quad \overline{\overline{\alpha}}_{\rm mm} = \begin{bmatrix} \alpha_{\rm mm}^{xx} & \alpha_{\rm mm}^{xy} & \alpha_{\rm mm}^{xz} \\ \alpha_{\rm mm}^{yx} & \alpha_{\rm mm}^{yy} & \alpha_{\rm mm}^{yz} \\ \alpha_{\rm mm}^{zx} & \alpha_{\rm mm}^{zy} & \alpha_{\rm mm}^{zz} \end{bmatrix}. \tag{8}$$

With substituting (2), (3), (7), and (8) into (4) and (5) and after some algebraic manipulations, the most general form for the copolarized reflection and transmission coefficients of the metasurface can be obtained as

$$R_{\pm}^{s\to s} = \frac{-j\omega}{2}\Bigg[\frac{\eta}{\cos\theta}\alpha_{\rm ee}^{yy} \pm \alpha_{\rm em}^{yx} \mp \tan\theta\alpha_{\rm em}^{yz} \mp \alpha_{\rm me}^{xy} - \frac{\cos\theta}{\eta}\alpha_{\rm mm}^{xx} + \frac{\sin\theta}{\eta}\alpha_{\rm mm}^{xz} \mp \tan\theta\alpha_{\rm me}^{zy} - \frac{\sin\theta}{\eta}\alpha_{\rm mm}^{zx} + \frac{\sin\theta\tan\theta}{\eta}\alpha_{\rm mm}^{zz}\Bigg] \tag{9}$$

$$T_{\pm}^{s\to s} = 1 - \frac{j\omega}{2}\Bigg[\frac{\eta}{\cos\theta}\alpha_{\rm ee}^{yy} \pm \alpha_{\rm em}^{yx} \mp \tan\theta\alpha_{\rm em}^{yz} \pm \alpha_{\rm me}^{xy} + \frac{\cos\theta}{\eta}\alpha_{\rm mm}^{xx} - \frac{\sin\theta}{\eta}\alpha_{\rm mm}^{xz} \mp \tan\theta\alpha_{\rm me}^{zy} - \frac{\sin\theta}{\eta}\alpha_{\rm mm}^{zx} + \frac{\sin\theta\tan\theta}{\eta}\alpha_{\rm mm}^{zz}\Bigg] \tag{10}$$

$$R_{\pm}^{p\to p} = \frac{-j\omega}{2}\Bigg[\eta\cos\theta\alpha_{\rm ee}^{xx} \mp \alpha_{\rm em}^{xy} - \eta\sin\theta\alpha_{\rm ee}^{xz} \pm \alpha_{\rm me}^{yx} - \frac{1}{\eta\cos\theta}\alpha_{\rm mm}^{yy} \mp \tan\theta\alpha_{\rm me}^{yz} + \eta\sin\theta\alpha_{\rm ee}^{zx} \mp \tan\theta\alpha_{\rm em}^{zy} - \eta\sin\theta\tan\theta\alpha_{\rm ee}^{zz}\Bigg] \tag{11}$$

$$T_{\pm}^{p\to p} = 1 - \frac{j\omega}{2}\Bigg[\eta\cos\theta\alpha_{\rm ee}^{xx} \mp \alpha_{\rm em}^{xy} - \eta\sin\theta\alpha_{\rm ee}^{xz} \mp \alpha_{\rm me}^{yx} + \frac{1}{\eta\cos\theta}\alpha_{\rm mm}^{yy} \pm \tan\theta\alpha_{\rm me}^{yz} - \eta\sin\theta\alpha_{\rm ee}^{zx} \pm \tan\theta\alpha_{\rm em}^{zy} + \eta\sin\theta\tan\theta\alpha_{\rm ee}^{zz}\Bigg]. \tag{12}$$

These equations reveal the angular dispersion behavior of the reflection and transmission coefficients for a nonreciprocal bianisotropic metasurface in its general form with 36 tonsorial components and will be instrumental for the discussions presented in the following.

B. Nonreciprocal On-Axis Differentiator

The main goal of this article is to search for the best group of polarizability components whereby the reflection or transmission coefficient in (9)–(12), $\tilde{\mathbf{R}}(\mathrm{k}_x)$ or $\tilde{\mathbf{T}}(\mathrm{k}_x)$, obeys the angular dispersion of the desired mathematical operator. The first-order differentiation operation is a good representative for the family of asymmetric OTFs. Referring to $\tilde{H}(\mathrm{k}_x) = \mathrm{j}\mathrm{k}_x$ for the first-order differentiation operator, our purpose is to realize an on-axis reflective channel whose TF, $\tilde{R}(\mathrm{k}_x)$, has indispensably a nonlocal odd-symmetric treatment around $\theta = 0$ without polarization rotation, i.e., $\mathrm{R}(\theta) = \mathrm{R}(-\theta)$. Let us consider the conceptual illustration of Fig. 1(b) in which the possibility of $\mathrm{R}(\theta) \neq \mathrm{R}(-\theta)$ is graphically investigated. A first-order, polarization-preserving, differentiation operation requires that the copolarized reflection coefficient imparted on the plane wave coming from $R_{2\to1}$ channel (θ illumination) essentially differs from that seen from $R_{1\to2}$ channel ($-\theta$ illumination), which is prohibited by reciprocity. Thus, resorting to a nonreciprocal metasurface is inevitable to implement a polarization-preserved first-order differentiator for on-axis illuminations [29]. This observation can be verified by (9) and (11) in which the necessary condition to keep terms with odd functionality from θ is $\alpha_{\rm em}^{yz} \neq -\alpha_{\rm me}^{zy}$ or $\alpha_{\rm mm}^{xz} \neq \alpha_{\rm mm}^{zx}$ for s-polarized incidences and $\alpha_{\rm ee}^{xz} \neq \alpha_{\rm ee}^{zx}$ or $\alpha_{\rm me}^{yz} \neq -\alpha_{\rm em}^{zy}$ for p-polarized incidences. These constraints for polarization-preserved reflective optical processing obviously break the Casimir–Onsager reciprocity relations [55]. However, as can be directly inferred from (10) and (12), polarization-preserving on-axis asymmetric OTFs in transmission regime can be simply implemented by using a reciprocal metasurface having nonzero $\alpha_{\rm mm}^{xz}$ and $\alpha_{\rm ee}^{xz}$ for s- and p-polarized incidences, respectively.

As a representative example, let us consider the following synthesis problem: find the surface polarizabilities of a nonreciprocal metasurface for which a p-polarized input field with an illumination angle of $\theta_{\rm inc} = 0°$ reflects into a copolarized beam whose profile is the first-order derivative of the one of the input. A Gaussian-shape beam profile with a spatial bandwidth of $W = 0.2k_0$ is considered as the input field. In order to obtain the required surface polarizabilties, the metasurface synthesis will be treated as a nonlinear optimization problem that is solved numerically. First, according to the scattering role of each polarizability component, the neutral components are assumed to be zero. The involved polarizabilities are $\alpha_{\rm ee}^{xx}$, $\alpha_{\rm ee}^{xz}$, $\alpha_{\rm ee}^{zx}$, $\alpha_{\rm ee}^{zz}$, and $\alpha_{\rm mm}^{yy}$. Then, we seek for those surface polarizabilities for which the difference between the desired GF, $\tilde{G}_{\rm des}(k_x) = \mathrm{j}\mathrm{k}_x$, and the angle-dependent reflection coefficient of the metasurface,

$$\overline{\overline{Z}} = \eta\begin{bmatrix} \cos\theta\cos^2\phi + \sin^2\phi/\cos\theta & (\cos\theta - 1/\cos\theta)\sin\phi\cos\phi \\ (\cos\theta - 1/\cos\theta)\sin\phi\cos\phi & \cos\theta\sin^2\phi + \cos^2\phi/\cos\theta \end{bmatrix} \tag{6}$$

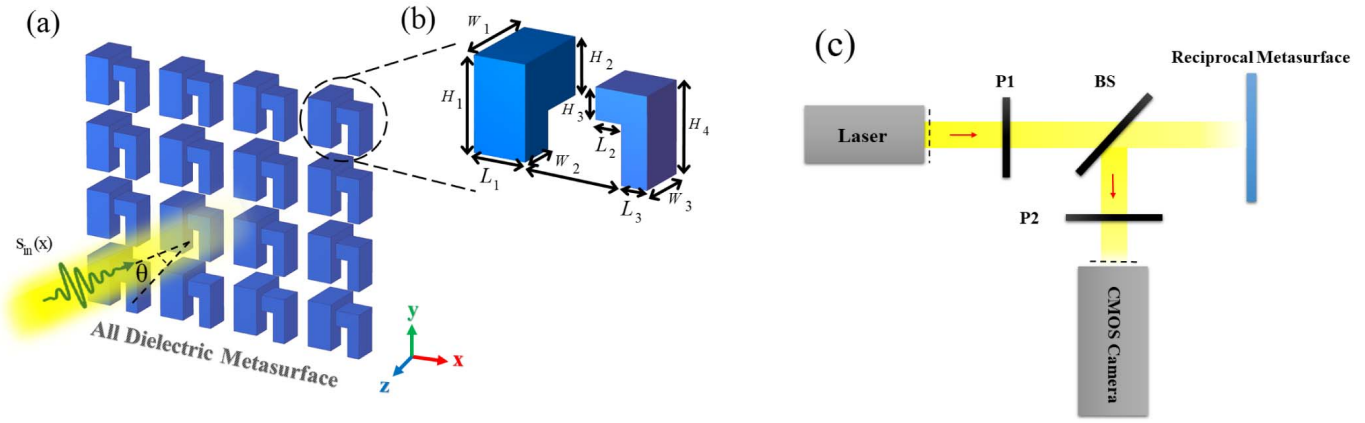

Fig. 3. (a) Array of polarizable meta-atoms for performing optical signal processing. (b) Proposed reciprocal bianisotropic meta-atom exposing normal polarizability components. The geometry was chosen in such a way that both symmetries in xy and yz planes are broken. The geometrical parameters are $L_1 = 410$ nm, $L_2 = 205$ nm, $L_3 = 205$ nm, $L_4 = 350$ nm, $w_1 = 695$ nm, $w_2 = 315$ nm, $w_3 = 410$ nm, $H_1 = 760$ nm, $H_2 = 455$ nm, $H_3 = 250$ nm, and $H_4 = 730$ nm. (c) Schematic setup for testing the optical signal processing performance of the reflective metasurface in which P and BS stand for the polarizer and beam splitter, respectively.

$\tilde{R}(k_x)$, is minimized within a predetermined angular range. The cost function is defined as the sum of squares of the differences at a finite number of N samples for both real and imaginary parts $f = w_{\text{re}}\sum_{i=1}^{N}\left(\text{Re}[\tilde{G}_{\text{des}}(k_{x,i}) - \tilde{R}(k_{x,i})]\right)^2 + w_{\text{im}}\sum_{i=1}^{N}\left(\text{Im}[\tilde{G}_{\text{des}}(k_{x,i}) - \tilde{R}(k_{x,i})]\right)^2$. Here, w_{re} and w_{im} represent the weight coefficients established to selectively adjust the contribution of real and imaginary parts, respectively. At this stage, the metasurface processor is synthesized with the optimized polarizabilities shown in Fig. 2. It should be noted that, since $\alpha_{\text{ee}}^{\text{xz}}$ is not equal to $\alpha_{\text{ee}}^{\text{zx}}$, the synthesized metasurface is nonreciprocal. The resultant TFs along with the input and output fields are shown in Fig. 2(a)–(c). These figures show good agreement between the desired and synthesized TFs and output beam profiles. Indeed, the reflected field propagating out along the boresight direction is the first-order derivative of the Gaussian-shape input field. The accuracy of differentiation is 99.5%, described by the Pearson correlation coefficient between the simulated and exact reflected field amplitudes. The results confirm that at the expense of a complex fabrication, a suitably designed nonreciprocal anisotropic metasurface can be thought of as a reflective optical first-order differentiator working for input fields coming from normal direction.

C. Reciprocal On-Axis Differentiator

As an alternative solution, incorporating cross-polarization channels to the problem can elaborately circumvent the nettlesome restrictions arising from reciprocity. In this case, the polarizability components are engineered so that the polarization state of the incident light coming from Port 1 is rotated when it is captured at Port 2 [see Fig. 1(b)]. Hereafter, the cross-polarized reflection of $R^{s\to p}$ or $R^{p\to s}$ serves as the TF of our processing channel, meaning that the output signal has orthogonal polarization with respect to that of the input wave. It should be noted that such a metasurface, if designed, will exhibit $R_{1\to 2}^{s\to p} \neq R_{2\to 1}^{s\to p}$, which no longer quashes the reciprocity condition. A similar deduction can be made for $R_{1\to 2}^{p\to s} \neq R_{2\to 1}^{p\to s}$. Due to the insensitivity of conventional optical sensors, including the human eyes, to the polarization of light, polarization rotation does not degrade the overall performance of optical differentiator; instead, it dramatically facilitates the realization procedure. Based on (2)–(8), the cross-polarized reflection and transmission coefficients of the metasurface read as

$$R^{s\to p} = \frac{-j\omega}{2}\Bigg[\eta\alpha_{\text{ee}}^{xy} \pm \cos\theta\alpha_{\text{em}}^{xx} \mp \sin\theta\alpha_{\text{em}}^{xz} \pm \frac{\alpha_{\text{me}}^{yy}}{\cos\theta} + \frac{1}{\eta}\alpha_{\text{mm}}^{yx} - \frac{\tan\theta}{\eta}\alpha_{\text{mm}}^{yz} + \eta\tan\theta\alpha_{\text{ee}}^{zy} \pm \sin\theta\alpha_{\text{em}}^{zx} \mp \sin\theta\tan\theta\alpha_{\text{em}}^{zz}\Bigg] \tag{13}$$

$$T^{s\to p} = -\frac{j\omega}{2}\Bigg[\eta\alpha_{\text{ee}}^{xy} \pm \cos\theta\alpha_{\text{em}}^{xx} \mp \sin\theta\alpha_{\text{em}}^{xz} \mp \frac{\alpha_{\text{me}}^{yy}}{\cos\theta} - \frac{1}{\eta}\alpha_{\text{mm}}^{yx} + \frac{\tan\theta}{\eta}\alpha_{\text{mm}}^{yz} - \eta\tan\theta\alpha_{\text{ee}}^{zy} \mp \sin\theta\alpha_{\text{em}}^{zx} \pm \sin\theta\tan\theta\alpha_{\text{em}}^{zz}\Bigg] \tag{14}$$

$$R^{p\to s} = \frac{-j\omega}{2}\Bigg[\eta\alpha_{\text{ee}}^{yx} \mp \frac{1}{\cos\theta}\alpha_{\text{em}}^{yy} - \eta\tan\theta\alpha_{\text{ee}}^{yz} \mp \cos\theta\alpha_{\text{me}}^{xx} + \frac{1}{\eta}\alpha_{\text{mm}}^{xy} \pm \sin\theta\alpha_{\text{me}}^{xz} \mp \sin\theta\alpha_{\text{me}}^{zx} + \frac{\tan\theta}{\eta}\alpha_{\text{mm}}^{zy} \pm \sin\theta\tan\theta\alpha_{\text{me}}^{zz}\Bigg] \tag{15}$$

$$T^{p\to s} = -\frac{j\omega}{2}\Bigg[\eta\alpha_{\text{ee}}^{yx} \mp \frac{1}{\cos\theta}\alpha_{\text{em}}^{yy} - \eta\tan\theta\alpha_{\text{ee}}^{yz} \pm \cos\theta\alpha_{\text{me}}^{xx} - \frac{1}{\eta}\alpha_{\text{mm}}^{xy} \mp \sin\theta\alpha_{\text{me}}^{xz} \mp \sin\theta\alpha_{\text{me}}^{zx} + \frac{\tan\theta}{\eta}\alpha_{\text{mm}}^{zy} \pm \sin\theta\tan\theta\alpha_{\text{me}}^{zz}\Bigg]. \tag{16}$$

It should be remembered that we are seeking for those reciprocal collective polarizability tensors, which can be potentially effective to satisfy two important conditions at the same time: exciting the cross-polarization reflected fields and making the

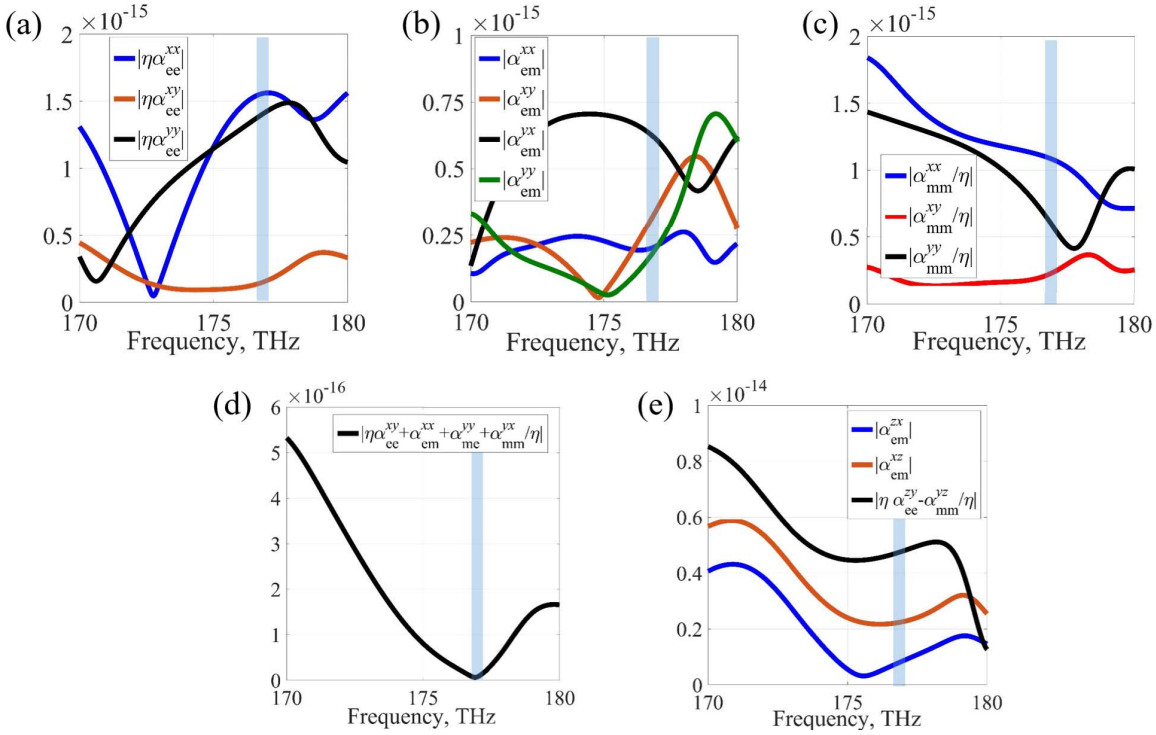

Fig. 4. (a)–(c) Tangential collective polarizabilties of the designed optical metasurface given in Fig. 3(a). Evaluation of (d) zero cross-polarized reflection and (e) asymmetric angular dispersion conditions on the surface polarizabilities. The working frequency is $f = 177$ THz and is highlighted by a blue marker in the figures.

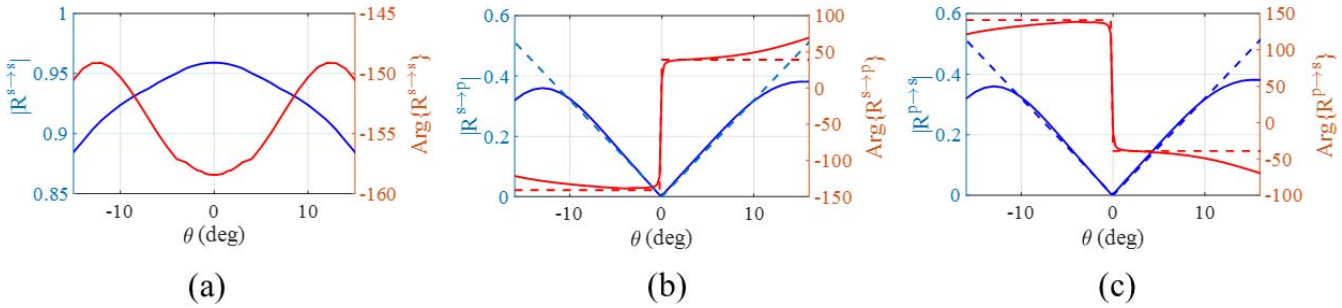

Fig. 5. Phase and amplitude of (a) copolarized and (b) s → p and (c) p → s reflection coefficients. The phase and amplitude of the exact TF for implementing the first-order differentiation operation are also presented. The solid and dashed lines stand for the exact and the synthesized TFs, respectively, and the working frequency is $f = 177$ THz.

cross-polarized reflection to be an asymmetric function of k_x (or θ) variable. As clearly seen from (13) and (15), although the presence of nine surface polarizabilities leads to the generation of cross-polarized reflection fields for each of s- and p-polarized illuminations, only four of them deal with odd-order terms (with respect to θ). Indeed, the necessary condition for reciprocal realization of on-axis asymmetric OTFs in the cross-polarized reflective channel is the presence of the following.

Rule I:

$\alpha_{\rm em}^{xz}$ or $\alpha_{\rm mm}^{yz}$ or $\alpha_{\rm ee}^{zy}$ or $\alpha_{\rm em}^{zx}$ (s-polarized illumination)
$\alpha_{\rm ee}^{yz}$ or $\alpha_{\rm me}^{xz}$ or $\alpha_{\rm me}^{zx}$ or $\alpha_{\rm mm}^{zy}$ (p-polarized illumination).

This means that the role of normal polarizabilities and bianisotropy is undeniable for a reciprocal metasurface to build asymmetric angular dispersion behavior for the reflection around $k_x = 0$. We call these surface polarizability components cross-polarization exciting normal polarizabilities (CPENPs) throughout this article. The cross-polarized transmission processing channel can also be enabled if the surface polarizabilities $\alpha_{\rm mm}^{yz}$ or $\alpha_{\rm ee}^{zy}$ for s-polarized illumination and $\alpha_{\rm ee}^{yz}$ or $\alpha_{\rm mm}^{zy}$ for p-polarized input signals contribute to the overall scattering of the metasurface. For the specular case of first-order differentiation operator, $R^{\rm cr}(k_x = 0) = 0$, meaning that no cross-polarized field should exist upon illuminating by on-axis plane waves. Mathematically speaking, (13) and (15) imply that the following condition holds:

Rule II:

$$\eta\alpha_{\rm ee}^{xy} \pm \alpha_{\rm em}^{xx} \pm \alpha_{\rm me}^{yy} + \frac{1}{\eta}\alpha_{\rm mm}^{yx} = 0 \quad \text{(s-polarized illumination)}$$

$$\eta\alpha_{\rm ee}^{yx} \mp \alpha_{\rm em}^{yy} \mp \alpha_{\rm me}^{xx} + \frac{1}{\eta}\alpha_{\rm mm}^{xy} = 0 \quad \text{(p-polarized illumination)}$$

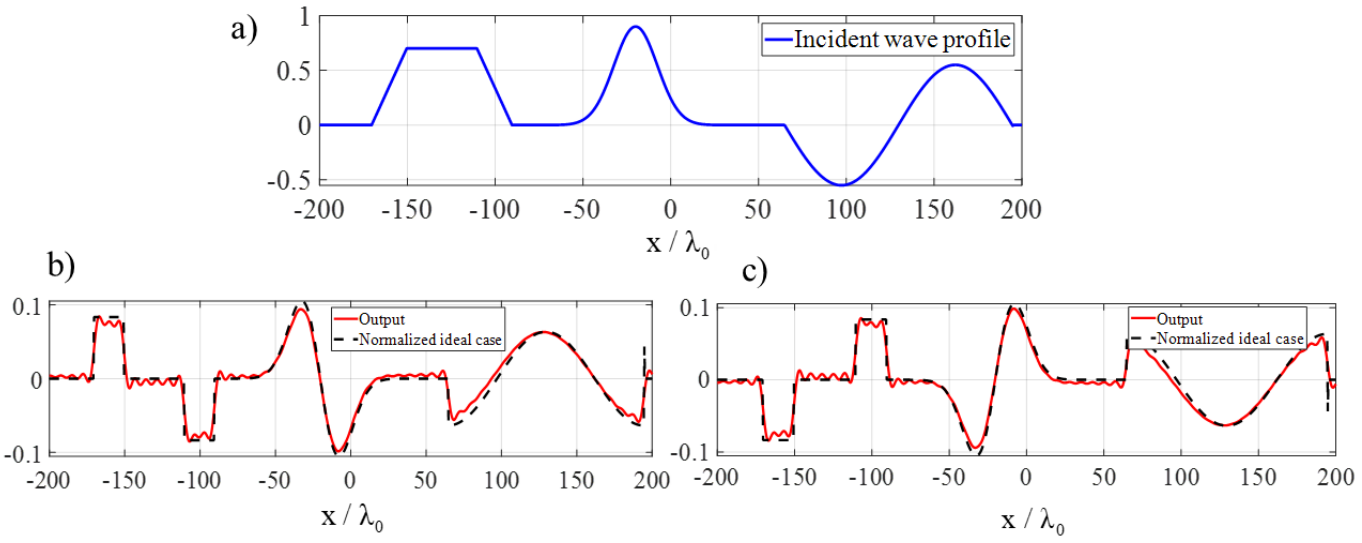

Fig. 6. (a) Field profile of the input signal, formed by a combination of trapezoidal, Gaussian, and sinusoidal functions. (b), and (c) s → p and p → s reflected field profiles, respectively. The exact derivative signals have also been presented for the sake of comparison. The metasurface is illuminated from normal direction and the working frequency is $f = 177$ THz.

which must be satisfied because, otherwise, the metasurface may expose nonzero cross-polarized reflection at $\theta = 0$. In summary, among all possible types of bianisotropy and longitudinal polarizabilities, specific solutions are desired, which have been comprehensively discussed above. As an important deduction from Fig. 1(b), the reciprocity enforces $R^{s\to p}(\theta) = R^{p\to s}(-\theta)$, meaning that the mirror version of each mathematical operator realized by $R^{s\to p}$ channel, $\tilde{H}(\mathrm{k}_x)$, will also be constructed by $R^{p\to s}$ channel, $\tilde{H}(-\mathrm{k}_x)$. Indeed, the proposed approach is inherently dual-polarized and can be applied to both s- and p-polarized input signals for many types of TFs such as spatial differentiation and integration for which $\tilde{H}(-\mathrm{k}_x)$ still yields a usable output wave. This interesting feature that has been rarely reported in the literature may find great potential applications in dual-polarized optical computations [17], [31].

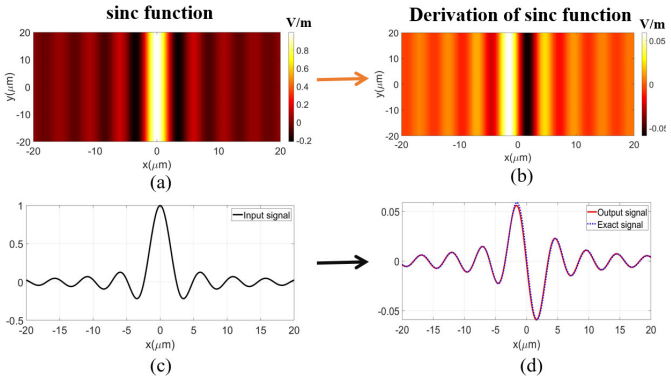

Fig. 7. (a) and (c) s-polarized sinc-shape incident field profile together with (b) and (d) p-polarized reflected derivative field profile. The exact derivative signals have also been presented for the sake of comparison. The reciprocal metasurface is illuminated from normal direction and the working frequency is $f = 177$ THz.

III. Dual-Polarized Optical Signal and Image Processing

As known, the macroscopic scattering features of any metasurface are mainly determined by properties of its constituent meta-atoms in the microscopic scale [50], [52]. In this section, we demonstrate that the proposed all-dielectric optical metasurface shown in Fig. 3(a) exposes the same collective polarizabilities required for performing first-order spatial differentiation at the macroscopic view. The meta-atom of Fig. 3(a) comprises two nonidentical L-shaped dielectric particles with a relative 90° rotation. The meta-atoms are made of silicon (Si) material whose relative permittivity is extracted from Palik's book [56]. A comprehensive parametric study has been accomplished to search for the best group of parameters making the angular dispersion of the cross-polarized reflection coefficient of the dielectric particles as close to the desired TF as possible. The dielectric inclusions are periodically repeated with the periodicity of 1.1 and 0.9 μm along both the x- and y-directions, respectively. The angular dependence of the scattering properties reflects the symmetry of the meta-atoms. There are three possible types of symmetries [34]: 180°-rotation symmetry around the y-axis (C2), reflection symmetry through the x-axis (σ_x), and reflection symmetry through the z-axis (σ_z). If the scattering particles do not exhibit any structural symmetry, then the resulting metasurface corresponds to a bianisotropic structure with both normal and tangential polarization densities and its angular scattering response does not present any symmetry in addition to those imposed by reciprocity [34], [51]. As a consequence, as shown in Fig. 3(b), we break the mentioned geometrical symmetries in order to obtain a reciprocal bianisotropic metasurface whose CPENP are effectively excited at oblique incidences.

Based on the retrieval procedure presented in [51] and [57], the in-plane collective polarizabilities of the designed metasurface have been extracted. In fact, after the dipole approximation of meta-atoms in a polarizability retrieval setup, the metasurface is illuminated by four normally incident plane waves, and the tangential polarizations can be described in

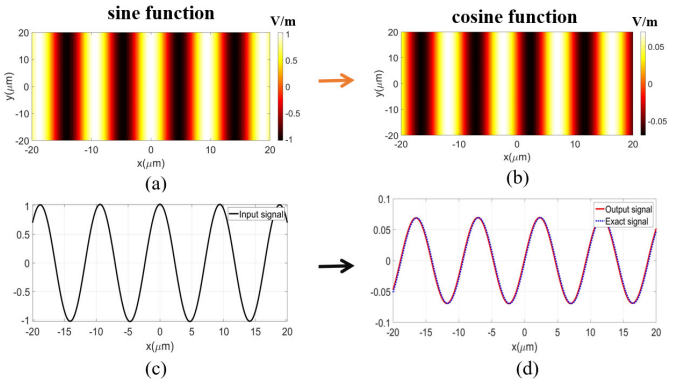

Fig. 8. (a) and (c) p-polarized sinc-shape incident field profile together with (b) and (d) s-polarized reflected derivative field profile. The exact derivative signals have also been presented for the sake of comparison. The reciprocal metasurface is illuminated from normal direction and the working frequency is $f = 177$ THz.

terms of induced dipole moments. By applying an equivalent surface model for the bianisotropic sheet, the *tangential* collective polarizabilities can be calculated as a function of the reflection/transmission coefficients from the array. The retrieved results are shown in Fig. 4(a)–(c). Moreover, the zero cross-polarized reflection condition of the surface polarizabilities at the normal incidence has been assessed in Fig. 4(d). As seen, rule II is satisfied in the vicinity of 177 THz at which the metasurface creates no on-axis cross-polarized fields at the reflection side. Hereafter, we intend to distinguish which one of the CPENP is provided by the designed metasurface. After some mathematical manipulations on (13) and (15) and with applying the reciprocity constraints, we have

$$\alpha_{\rm em}^{xz} = -\alpha_{\rm me}^{zx} = \frac{1}{j2\omega\sin\theta} \times \left[\left(R_{\theta,+}^{s\to p} - R_{-\theta,+}^{s\to p}\right) + \left(T_{\theta,+}^{s\to p} - T_{-\theta,+}^{s\to p}\right)\right] \tag{17}$$

$$\alpha_{\rm em}^{zx} = -\alpha_{\rm me}^{xz} = \frac{1}{-j2\omega\sin\theta} \times \left[\left(R_{\theta,+}^{s\to p} - R_{-\theta,+}^{s\to p}\right) + \left(T_{\theta,-}^{s\to p} - T_{-\theta,-}^{s\to p}\right)\right] \tag{18}$$

$$\eta\alpha_{\rm ee}^{zy} - \frac{1}{\eta}\alpha_{\rm mm}^{yz} = \frac{1}{-j2\omega\tan\theta} \times \left[\left(R_{\theta,+}^{s\to p} - R_{\theta,-}^{s\to p}\right) - \left(T_{\theta,+}^{s\to p} - T_{\theta,-}^{s\to p}\right)\right]. \tag{19}$$

Four s-polarized oblique plane waves illuminating the metasurface along the forward and backward directions serve to extract some information regarding the normal components of the collective polarizabilities. By using an arbitrary small incident wave angle $\theta = 4°$, all required scattering parameters in (17)–(19) have been simulated and the left-hand side parameters are plotted in Fig. 4(e). As can be seen, the results clearly demonstrate that around 177 THz, among eight possible CPENP, the impact of $\eta\alpha_{\rm ee}^{zy} - (1/\eta)\alpha_{\rm mm}^{yz}$ is more tangible, while the role of $\alpha_{\rm em}^{zx}$ can be neglected. Indeed, the engineered geometry of the designed reciprocal meta-atom makes it as a suitable choice for realizing on-axis asymmetric OTFs in the reflection side.

For instance, the cross-polarized reflection coefficient of the array can be tailored to mimic the angular trend of $\mathrm{R}^{s\to p}(\theta) = j\zeta\sin(\theta)$. The parameter ζ stands for the gain of differentiator, which depends on the value of surface polarizabilites. Through engineering the meta-atom geometry, one can achieve a cross-polarized response that approximates the nonlocal behavior of the first-derivative operation with a phase jump at $\mathrm{k}_x = 0$. The phase and amplitude of the copolarized and cross-polarized reflection coefficients at $f = 177$ THz are plotted in Fig. 5(a)–(c). The results are numerically recorded by using CST full-wave commercial software, where periodic boundary conditions are applied to the x- and y-directed walls and Floquet ports are considered along the z-direction. The first deduction is that the copolarized reflection coefficient possesses a symmetric response with respect to k_x due to the reciprocity theorem [see Fig. 5(a)]. The second inference is that, as expected from the presented analysis, the cross-polarized reflection for both s- and p-polarized incidences, possesses an odd-symmetric spatial trend around $\mathrm{k}_x = 0$. Due to the reciprocity constraint and $\tilde{R}^{s\to p}(k_x) = -\tilde{R}^{s\to p}(-k_x)$, the results of Fig. 5(b) and (c) differ only in the phase sign. The exact amplitude and phase of the TF representing the first-order differentiation operation are fairly compared with those synthesized by the designed metasurface. An excellent agreement between the cross-polarization reflection of the designed metasurface and the exact TF has been achieved as long as the normalized spatial bandwidth of the input signals lies within $|k_x/k_0| < 0.25$. This range essentially provides the maximum spatial resolution of input signals that can be correctly processed by the designed optical metasurface. It should be noted that the effects of losses are included in the numerical results. They are modeled by a nonzero imaginary part in the dielectric constant of silicon. Moreover, due to the intrinsic $\chi^{(3)}$ nonlinear behavior of silicon, the optical response of the designed meta-atom slightly changes in the case of extremely high optical intensities. In fact, the first-order correction due to the nonlinear Kerr effect is a dependence of the refractive index to the optical intensity, i.e., $\varepsilon = \varepsilon_{lin} + \chi^{(3)}|E|^2$ and $\chi^{(3)} = 2.8 \times 10^{-18}$ m^2/V^2 [58]. Since $\chi^{(3)}$ is small, the nonlinear effects only appear when the optical intensity is very large. Our simulations confirm that the performance of the signal/image processing predicted by the linear limit is not deteriorated as long as the optical intensity remains below tens of GW/cm^2. Therefore, optical signal processing can be safely performed without being affected by nonlinear effects, even at moderate intensity levels.

To inspect the differentiation performance of the employed metasurafce processor, a complex signal that is a combination of trapezoidal, Gaussian, and sinusoidal functions [see Fig. 6(a)] has been utilized as the beam profile of the on-axis incidence. The details for the schematic setup are shown in Fig. 3(c). The polarizers are utilized to filter out the unwanted polarization in each case and the beam splitter is aimed at directing the reflected fields to the camera. The cross-polarized reflections egressing the metasurface from s $\to$ p and p $\to$ s normal processing channels are captured as output signals and the corresponding results are shown Fig. 6(b) and (c), respectively. The output signals were in this

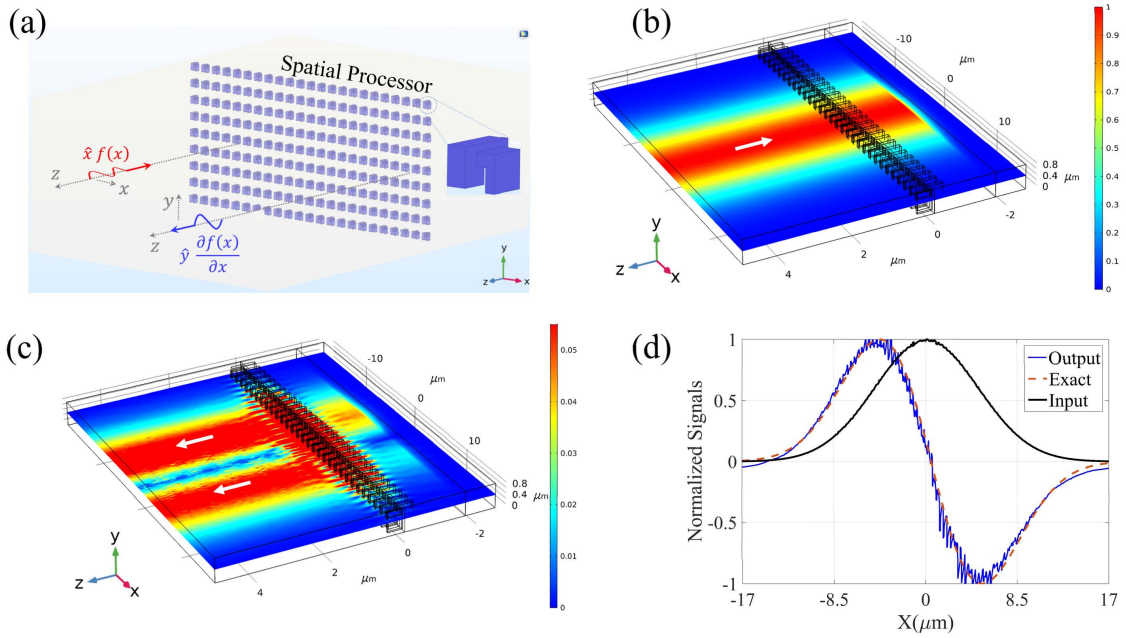

Fig. 9. 3-D full-wave simulation for verification of the proposed on-axis differentiation method. (a) Finite array of all-dielectric meta-atoms. (b) Intensity of the x-polarized incident field (input signal). (c) Intensity of the y-polarized reflected field (output signal). (d) Comparison between the cross-polarized reflected field and the exact derivative of the input signal at the distance $5\lambda_0$ from the bianisotropic metasurface.

manner: Each plane-wave impinging on the metasurface will be reflected with a certain reflection coefficient corresponding to its incident wave angle, $\tilde{R}(k_x)$. In this case, the angular spectrum of the output fields is given by

$$\tilde{g}_{\text{ch1}}(k_x) = \tilde{R}^{s\to p}(k_x)\,\tilde{f}_{\text{ch1}}(k_x) \tag{20}$$

$$\tilde{g}_{\text{ch2}}(k_x) = \tilde{R}^{p\to s}(k_x)\,\tilde{f}_{\text{ch2}}(k_x) \tag{21}$$

in reflection mode. Here, the subscripts denote the number of processing channel. Thus, the synthesized output fields can be numerically calculated as

$$E_{\text{ref, ch1}} = \int_{k_{0x}-W}^{k_{0x}+W} \tilde{R}^{s\to p}(k_x)\,\tilde{f}_{\text{ch1}}(k_x)\,\exp\left(-jk_x x - jk_z z\right) dk_x \tag{22}$$

$$E_{\text{ref, ch2}} = \int_{k_{0x}-W}^{k_{0x}+W} \tilde{R}^{p\to s}(k_x)\,\tilde{f}_{\text{ch2}}(k_x)\,\exp\left(-jk_x x - jk_z z\right) dk_x. \tag{23}$$

As can be seen, the all-dielectric optical metasurface successfully implements the first-order differentiation of the input signal at both output terminations. Indeed, when the input signal is reflected by the metasurface, the flat regimes are filtered out, the linear segments are converted to flat ones, the sine is converted to the cosine one, and finally, the descending and ascending parts of the Gaussian signal are distinguished. To evaluate the performance of our metasurface differentiator, the numerically obtained results are compared with the exact first-derivative of the input signals in the same figures. The results are exactly the responses expected from a first-derivative operation with only 2% error according to $e_f = (\|s_{\text{out}}^{\text{exact}}(x) - s_{\text{out}}^{\text{simul}}(x)\|)/\|s_{\text{out},x}^{\text{ideal}}(x)\|$. Therefore, the effective role of CPENP in constructing odd-symmetric nonlocal reflection suggests a new reciprocal way to realize first-order spatial differentiation for normal illuminations. It should be mentioned that the designed metasurface is suitable for optical applications [35].

The metasurface processor is dual-polarized and the processing channel can also carry a couple of input–output signals, separately. Two distinct 1-D signals (sinc and sinusoidal functions) representing the beam profiles of s- and p-polarized on-axis incidences are considered as the input signals [see Figs. 7(a) and (c) and 8(a) and (c)]. As shown in Figs. 7(b) and (d) and 8(b) and (d), both orthogonal channels can separately serve to construct the first-order derivative of the corresponding input fields at the output termination.

To further verify the performance of the proposed metasurface differentiator, 3-D full-wave simulations have been carried out (COMSOL Multiphysics). An x-polarized Gaussian beam is normally incident on the array of meta-atoms. The medium surrounding the bianisotropic metasurface is filled by air. The boundary conditions are selected as perfectly matched layers (PMLs) and periodic along the x- and y-directions, respectively. Fig. 9(a) and (b) shows the intensity of the incident field and the cross-polarized reflected field, respectively. Moreover, Fig. 9(c) shows a cutline of the normalized reflected field at a distance $5\lambda_0$ from the bianisotropic metasurface. The result of the full-wave simulation is compared with the exact first-order derivative of the input signal. As noticed, an excellent agreement has been obtained. More particularly, the positive and negative slopes of the input signal are clearly revealed in the cross-polarized reflected fields.

IV. Conclusion

To conclude, for the first time, we exploited the full macroscopic potential of a reciprocal bianisotropic metasurface to realize dual-polarized asymmetric OTFs at on-axis reflective processing channels. We analytically demonstrated how the cross-polarization channel governed by the CPENP can simply break the angular reflection of the metasurface

around $\theta = 0$ and mimic the k_x-asymmetric spatially dispersive TFs. Motivated by the existing relation between the angular scattering and geometrical mirror symmetries in the microscopic scale, the realization possibility of the proposed design was assessed through proposing an all-dielectric meta-atom and retrieving its important surface polarizabilities. The numerical simulations illustrated that the proposed metasurface reflects the first-derivative of the input signals, with either *s* or *p* polarization, coming from the normal direction, without using any bulky Fourier lens. The analytical design method presented in this article can be extended to 2-D scenarios by involving k_y wavenumber into the relations and obtaining explicit or implicit expression for $\tilde{R}(k_x, k_y)$. Therefore, the designed all-dielectric metasurface offers a simple and ultrathin normally oriented channel to perform optical signal/image processes without complicated settings arising from oblique illuminating setups or resorting to nonreciprocal media. Meanwhile, the proposed reflective processing system is more compatible with the current demands on the integrated devices than the transmissive ones while offering a promising vision for realizing parallel computations using both reflection and transmission channels.

REFERENCES

[1] J. W. Goodman, *Introduction to Fourier Optics*. Englewood, CO, USA: Robert & Company Publishers, 2005.

[2] H. Stark, *Application of Optical Fourier Transforms*. Amsterdam, The Netherlands: Elsevier, 2012.

[3] D. Mendlovic and H. M. Ozaktas, "Fractional Fourier transforms and their optical implementation: I," *JOSA A*, vol. 10, no. 9, pp. 1875–1881, 1993.

[4] J. Nakamura, *Image Sensors and Signal processing for Digital Still Cameras*. Boca Raton, FL, USA: CRC Press, 2017.

[5] A. Bogoni, L. Poti, R. Proietti, G. Meloni, F. Ponzini, and P. Ghelfi, "Regenerative and reconfigurable all-optical logic gates for ultra-fast applications," *Electron. Lett.*, vol. 41, no. 7, pp. 435–436, Mar. 2005.

[6] L. Brzozowski and E. H. T. Sargent, "All-optical analog-to-digital converters, hardlimiters, and logic gates," *J. Lightw. Technol.*, vol. 19, no. 1, p. 114, 2001.

[7] J. McGeehan, M. Giltrelli, and A. Willner, "All-optical digital 3-input AND gate using sum-and difference-frequency generation in PPLN waveguide," *Electron. Lett.*, vol. 43, no. 7, pp. 409–410, 2007.

[8] J. Xu, X. Zhang, J. Dong, D. Liu, and D. Huang, "All-optical differentiator based on cross-gain modulation in semiconductor optical amplifier," *Opt. Lett.*, vol. 32, no. 20, pp. 3029–3031, 2007.

[9] M. A. Al-Alaoui, "Novel digital integrator and differentiator," *Electron. Lett.*, vol. 29, no. 4, pp. 376–378, Feb. 1993.

[10] N. P. Jouppi *et al.*, "In-datacenter performance analysis of a tensor processing unit," in *Proc. 44th Annu. Int. Symp. Comput. Archit.*, 2017, pp. 1–12.

[11] A. Silva, F. Monticone, G. Castaldi, V. Galdi, A. Alù, and N. Engheta, "Performing mathematical operations with metamaterials," *Science*, vol. 343, no. 6167, pp. 160–163, Jan. 2014.

[12] F. Zangeneh-Nejad, D. L. Sounas, A. Alù, and R. Fleury, "Analogue computing with metamaterials," *Nature Rev. Mater.*, pp. 1–19, Oct. 2020.

[13] A. Pors, M. G. Nielsen, and S. I. Bozhevolnyi, "Analog computing using reflective plasmonic metasurfaces," *Nano Lett.*, vol. 15, no. 1, pp. 791–797, Jan. 2015.

[14] T. Zhu *et al.*, "Plasmonic computing of spatial differentiation," *Nature Commun.*, vol. 8, no. 1, p. 15391, Aug. 2017.

[15] H. Kwon, D. Sounas, A. Cordaro, A. Polman, and A. Alù, "Nonlocal metasurfaces for optical signal processing," *Phys. Rev. Lett.*, vol. 121, no. 17, Oct. 2018, Art. no. 173004.

[16] J. Zhou *et al.*, "Optical edge detection based on high-efficiency dielectric metasurface," *Proc. Nat. Acad. Sci. USA*, vol. 116, no. 23, pp. 11137–11140, Jun. 2019.

[17] H. Kwon, A. Cordaro, D. Sounas, A. Polman, and A. Alù, "Dual-polarization analog 2D image processing with nonlocal metasurfaces," *ACS Photon.*, vol. 7, no. 7, pp. 1799–1805, Jul. 2020.

[18] A. Youssefi, F. Zangeneh-Nejad, S. Abdollahramezani, and A. Khavasi, "Analog computing by brewster effect," *Opt. Lett.*, vol. 41, no. 15, pp. 3467–3470, 2016.

[19] D. A. Bykov *et al.*, "First-order optical spatial differentiator based on a guided-mode resonant grating," *Opt. Exp.*, vol. 26, no. 8, pp. 10997–11006, 2018.

[20] T. Zhu *et al.*, "Generalized spatial differentiation from the spin Hall effect of light and its application in image processing of edge detection," *Phys. Rev. A, Gen. Phys.*, vol. 11, no. 3, Mar. 2019, Art. no. 034043.

[21] C. Guo, M. Xiao, M. Minkov, Y. Shi, and S. Fan, "Photonic crystal slab Laplace operator for image differentiation," *Optica*, vol. 5, no. 3, pp. 251–256, 2018.

[22] N. M. Estakhri, B. Edwards, and N. Engheta, "Inverse-designed metastructures that solve equations," *Science*, vol. 363, no. 6433, pp. 1333–1338, Mar. 2019.

[23] F. Zangeneh-Nejad and R. Fleury, "Topological analog signal processing," *Nature Commun.*, vol. 10, no. 1, pp. 1–10, Dec. 2019.

[24] Y. Zhou, W. Wu, R. Chen, W. Chen, R. Chen, and Y. Ma, "Analog optical spatial differentiators based on dielectric metasurfaces," *Adv. Opt. Mater.*, vol. 8, no. 4, Feb. 2020, Art. no. 1901523.

[25] S. Abdollahramezani, O. Hemmatyar, and A. Adibi, "Meta-optics for spatial optical analog computing," *Nanophotonics*, vol. 9, no. 13, pp. 4075–4095, Sep. 2020.

[26] A. Abdolali, A. Momeni, H. Rajabalipanah, and K. Achouri, "Parallel integro-differential equation solving via multi-channel reciprocal bianisotropic metasurface augmented by normal susceptibilities," *New J. Phys.*, vol. 21, no. 11, Nov. 2019, Art. no. 113048.

[27] L. Wan *et al.*, "Optical analog computing of spatial differentiation and edge detection with dielectric metasurfaces," *Opt. Lett.*, vol. 45, no. 7, pp. 2070–2073, 2020.

[28] Y. Zhou, H. Zheng, I. I. Kravchenko, and J. Valentine, "Flat optics for image differentiation," *Nature Photon.*, vol. 14, no. 5, pp. 316–323, May 2020.

[29] A. Momeni, H. Rajabalipanah, A. Abdolali, and K. Achouri, "Generalized optical signal processing based on multioperator metasurfaces synthesized by susceptibility tensors," *Phys. Rev. A, Gen. Phys.*, vol. 11, no. 6, Jun. 2019, Art. no. 064042.

[30] T. J. Davis, F. Eftekhari, D. E. Gómez, and A. Roberts, "Metasurfaces with asymmetric optical transfer functions for optical signal processing," *Phys. Rev. Lett.*, vol. 123, no. 1, Jul. 2019, Art. no. 013901.

[31] A. Babaee, A. Momeni, A. Abdolali, and R. Fleury, "Parallel analog computing based on a 2×2 multiple-input multiple-output metasurface processor with asymmetric response," *Phys. Rev. A, Gen. Phys.*, vol. 15, no. 4, Apr. 2021, Art. no. 044015.

[32] A. Babaee, A. Momeni, M. M. Moeini, R. Fleury, and A. Abdolali, "Parallel optical spatial signal processing based on 2×2 MIMO computational metasurface," in *Proc. 14th Int. Congr. Artif. Mater. Novel Wave Phenomena (Metamaterials)*, Sep. 2020, pp. 195–197.

[33] A. Momeni, M. Safari, A. Abdolali, N. P. Kherani, and R. Fleury, "Asymmetric metal-dielectric metacylinders and their potential applications from engineering scattering patterns to spatial optical signal processing," *Phys. Rev. A, Gen. Phys.*, vol. 15, no. 3, Mar. 2021, Art. no. 034010.

[34] K. Achouri and O. J. F. Martin, "Angular scattering properties of metasurfaces," *IEEE Trans. Antennas Propag.*, vol. 68, no. 1, pp. 432–442, Jan. 2020.

[35] T. Niemi, A. O. Karilainen, and S. A. Tretyakov, "Synthesis of polarization transformers," *IEEE Trans. Antennas Propag.*, vol. 61, no. 6, pp. 3102–3111, Jun. 2013.

[36] E. F. Kuester, M. A. Mohamed, M. Piket-May, and C. L. Holloway, "Averaged transition conditions for electromagnetic fields at a metafilm," *IEEE Trans. Antennas Propag.*, vol. 51, no. 10, pp. 2641–2651, Oct. 2003.

[37] C. L. Holloway, E. F. Kuester, J. A. Gordon, J. O'Hara, J. Booth, and D. R. Smith, "An overview of the theory and applications of metasurfaces: The two-dimensional equivalents of metamaterials," *IEEE Antennas Propag. Mag.*, vol. 54, no. 2, pp. 10–35, Apr. 2012.

[38] A. Arbabi, E. Arbabi, Y. Horie, S. M. Kamali, and A. Faraon, "Planar metasurface retroreflector," *Nature Photon.*, vol. 11, no. 7, p. 415, 2017.

[39] A. Momeni, K. Rouhi, H. Rajabalipanah, and A. Abdolali, "An information theory-inspired strategy for design of re-programmable encrypted graphene-based coding metasurfaces at terahertz frequencies," *Sci. Rep.*, vol. 8, no. 1, pp. 1–13, Dec. 2018.

[40] K. Rouhi, H. Rajabalipanah, and A. Abdolali, "Real-time and broadband terahertz wave scattering manipulation via polarization-insensitive conformal graphene-based coding metasurfaces," *Annalen der Physik*, vol. 530, no. 4, Apr. 2018, Art. no. 1700310.

[41] M. Kiani, M. Tayarani, A. Momeni, H. Rajabalipanah, and A. Abdolali, "Self-biased tri-state power-multiplexed digital metasurface operating at microwave frequencies," *Opt. Exp.*, vol. 28, no. 4, pp. 5410–5422, 2020.

[42] M. Kiani, A. Momeni, M. Tayarani, and C. Ding, "Spatial wave control using a self-biased nonlinear metasurface at microwave frequencies," *Opt. Exp.*, vol. 28, no. 23, pp. 35128–35142, 2020.

[43] H. Rajabalipanah, A. Abdolali, J. Shabanpour, A. Momeni, and A. Cheldavi, "Asymmetric spatial power dividers using phase–amplitude metasurfaces driven by huygens principle," *ACS Omega*, vol. 4, no. 10, pp. 14340–14352, 2019.
[44] S. E. Hosseininejad, K. Rouhi, M. Neshat, A. Cabellos-Aparicio, S. Abadal, and E. Alarcón, "Digital metasurface based on graphene: An application to beam steering in terahertz plasmonic antennas," *IEEE Trans. Nanotechnol.*, vol. 18, pp. 734–746, 2019.
[45] S. E. Hosseininejad *et al.*, "Reprogrammable graphene-based metasurface mirror with adaptive focal point for THz imaging," *Sci. Rep.*, vol. 9, no. 1, pp. 1–9, Dec. 2019.
[46] R. Kargar, K. Rouhi, and A. Abdolali, "Reprogrammable multifocal THz metalens based on metal–insulator transition of VO2-assisted digital metasurface," *Opt. Commun.*, vol. 462, May 2020, Art. no. 125331.
[47] C. Pfeiffer and A. Grbic, "Metamaterial Huygens' surfaces: Tailoring wave fronts with reflectionless sheets," *Phys. Rev. Lett.*, vol. 110, no. 19, May 2013, Art. no. 197401.
[48] M. Selvanayagam and G. V. Eleftheriades, "Circuit modeling of huygens surfaces," *IEEE Antennas Wireless Propag. Lett.*, vol. 12, pp. 1642–1645, 2013.
[49] K. Achouri, M. A. Salem, and C. Caloz, "General metasurface synthesis based on susceptibility tensors," *IEEE Trans. Antennas Propag.*, vol. 63, no. 7, pp. 2977–2991, Jul. 2015.
[50] K. Achouri and C. Caloz, "Design, concepts, and applications of electromagnetic metasurfaces," *Nanophotonics*, vol. 7, no. 6, pp. 1095–1116, Jun. 2018.
[51] M. Yazdi and M. Albooyeh, "Analysis of metasurfaces at oblique incidence," *IEEE Trans. Antennas Propag.*, vol. 65, no. 5, pp. 2397–2404, May 2017.
[52] M. Albooyeh, S. Tretyakov, and C. Simovski, "Electromagnetic characterization of bianisotropic metasurfaces on refractive substrates: General theoretical framework," *Annalen der Physik*, vol. 528, nos. 9–10, pp. 721–737, Oct. 2016.
[53] M. Safari, A. Momeni, A. Abdolali, and N. P. Kherani, "Electric dipole-free meta-cylinders," in *Proc. 44th Int. Conf. Infr., Millim., THz Waves (IRMMW-THz)*, Sep. 2019, pp. 1–2.
[54] S. Tretyakov, *Analytical Modeling in Applied Electromagnetics*. Norwood, MA, USA: Artech House, 2003.
[55] A. Serdiukov, I. Semchenko, S. Tertyakov, and A. Sihvola, *Electromagnetics of Bi-Anisotropic Materials-Theory and Application*, vol. 11. Amsterdam, The Netherlands: Gordon and Breach Science, 2001.
[56] E. D. Palik and G. Ghosh, *Electronic Handbook of Optical Constants of Solids: User Guide*. New York, NY, USA: Academic, 1999.
[57] M. Yazdi and N. Komjani, "Polarizability calculation of arbitrary individual scatterers, scatterers in arrays, and substrated scatterers," *J. Opt. Soc. Amer. B, Opt. Phys.*, vol. 33, no. 3, pp. 491–500, 2016.
[58] D. L. Sounas and A. Alù, "Fundamental bounds on the operation of Fano nonlinear isolators," *Phys. Rev. B, Condens. Matter*, vol. 97, no. 11, Mar. 2018, Art. no. 115431.

Ali Momeni received the B.Sc. degree in electrical engineering from the Shiraz University of Technology, Shiraz, Iran, in 2016, and the M.Sc. degree in electrical engineering from the Iran University Science and Technology, Tehran, Iran, in 2019.

In 2020, he joined the Laboratory of Wave Engineering (LWE), École Polytechnique Fédérale de Lausanne (EPFL), Lausanne, Switzerland, as a Ph.D. student. He is currently working on the dispersive, active, and time-modulated metamaterial, metasurfaces, applied optics, advanced optical information processing, and optical machine learning.

Hamid Rajabalipanah was born in Tehran, Iran, in 1993. He received the B.Sc. and M.Sc. degrees in electrical engineering from the Iran University of Science and Technology, Tehran, in 2014 and 2016, respectively, where he is currently pursuing the Ph.D. degree in electrical engineering.

His current research interests include electromagnetic surfaces and applied electromagnetics.

Mahdi Rahmanzadeh was born in Amol, Iran, in 1994. He received the B.Sc. degree in electrical engineering from the Babol Noshirvani Institute of Technology, Babol, Iran, in 2015, and the M.Sc. degree in electrical engineering from the Iran University Science and Technology, Tehran, Iran, in 2018. He is currently pursuing the Ph.D. degree in electrical engineering with the Department of Electrical Engineering, Sharif University of Technology, Sharif, Iran.

His current research interests include electromagnetics, metamaterials, graphene metasurfaces, and photonics.

Ali Abdolali was born in Tehran, Iran, in 1974. He received the B.Sc. degree from the University of Tehran, Tehran, in 1998, the M.Sc. degree from the University of Tarbiat Modares, Tehran, in 2000, and the Ph.D. degree from the Iran University of Science and Technology (IUST), Tehran, in 2010, all in electrical engineering.

He joined the Department of Electrical Engineering, IUST, where he is currently an Associate Professor of electromagnetic engineering. He has authored or coauthored over 70 articles in international journals and conferences. His current research interests include electromagnetic wave scattering, radar cross section and RCSR, radar absorbing materials, cloaking, metamaterials, and wave propagation in complex media (anisotropic, inhomogeneous, and dispersive media), frequency-selective surfaces, and bioelectromagnetic.

Karim Achouri received the B.Sc. degree in microengineering and the M.Sc. degree in photonics and applied optics, as well as a minor in space technologies, from the Swiss Federal Institute of Technology in Lausanne (EPFL), Lausanne, Switzerland, in 2010 and 2012, respectively, and the Ph.D. degree in electromagnetics from the Polygrames Research Center, Ecole Polytechnique de Montréal, Montreal, QC, Canada, in 2017.

In 2013, he joined the Polygrames Research Center, Ecole Polytechnique de Montréal. In 2017, he joined the Nanophotonics and Metrology Laboratory (NAM), EPFL, as a Post-Doctoral Fellow. He is currently working on the mathematical synthesis, numerical analysis, and practical realization of optical metasurfaces. His research interests are in the areas of electromagnetics, metamaterials, applied optics, photonics, and nanotechnologies.

Viktar S. Asadchy was born in Gomel, Belarus, in 1990. He received the Diploma and master's degrees in physics from Gomel State University, Gomel, in 2013 and 2014, respectively, and the Doctor of Science degree from Aalto University, Aalto, Finland, in 2017.

He is currently working as a Post-Doctoral Fellow at the Department of Electrical Engineering, Stanford University, Stanford, CA, USA. His main research interests include spatially dispersive media, Weyl semimetals, metasurfaces, nonreciprocity, and advanced diffractive optical components.

Romain Fleury received the M.S. degree in micro and nanotechnology from the University of Lille, Lille, France, in 2010, and the Ph.D. degree in electrical and computer engineering from the University of Texas at Austin, Austin, TX, USA, in 2015.

He is a tenure-track Assistant Professor with the Institute of Electrical Engineering, Swiss Federal Institute of Technology in Lausanne (EPFL), Lausanne, Switzerland, and currently leads the EPFL Laboratory of Wave Engineering. In 2016, he was a Marie-Curie Post-Doctoral Fellow at ESPCI ParisTech, and the CNRS Langevin Institute, Paris, France. His research interests include a wide variety of topics in the field of wave physics and engineering, including periodic structures, active and time-modulated metamaterials, nonreciprocal wave propagation, classical topological insulators, nonlinear effects, and parity-time symmetry.